

Related to the letter entitled *Transport measurements across a tunable potential barrier in graphene* by B. Huard, J.A. Sulpizio, N. Stander, K. Todd, B. Yang and D. Goldhaber-Gordon published in Physical Review Letters

SUPPLEMENTARY MATERIAL

1. IMAGING, RAMAN SPECTROSCOPY, AND IDENTIFICATION OF SINGLE-LAYER GRAPHENE

After micromechanical cleavage and deposition of graphitic flakes onto a 280 nm thermally-grown oxide on Si, optical microscopy was used to identify the thinnest flakes [Geim and Novoselov(2007)]. Microscope settings (brightness, contrast, color balance) were tuned so that these thinnest flakes, presumed to be few- or single-layer graphene, could be consistently identified as verified by measurements with atomic force microscope and 3D white-light interferometry (using a profiler from Zygo corp.).

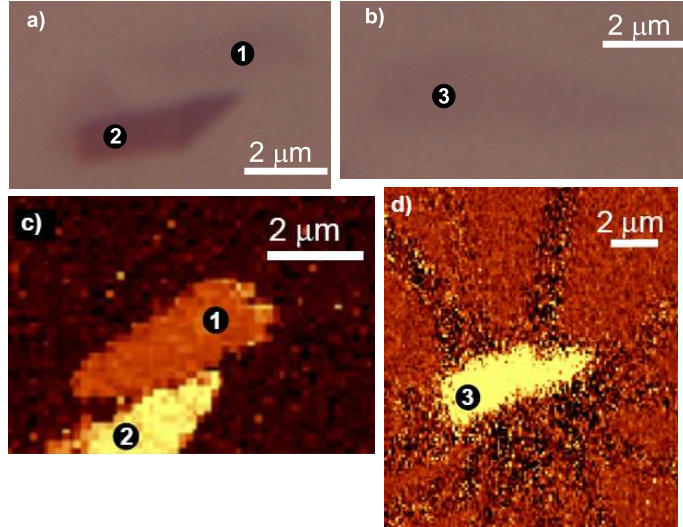


FIGURE 1. a) Optical image of nearby graphitic flake with labeled thin region 1 and thick region 2. b) Optical image of bare graphene sheet (labeled region 3) used to create the top-gated device described in the letter. Note the strong color similarity between the barely visible regions 1 and 3, suggesting the graphene thickness in these regions is close. c) Spatial map of the width of the $2D$ peak for regions 1 and 2. Region 1 appears less bright than region 2, indicating a narrower $2D$ peak and thinner graphene. d) Spatial map of $2D$ peak width for region 3. The color scale has been chosen differently from c) in order to see the Au contacts appear as dark lines.

An optical image of the bare graphene sheet studied in the letter after deposition on the oxide and before any further fabrication is shown in region ③ of Fig. 1b. As a comparison, Fig 1a shows a similar optical image of a nearby graphitic flake which consists of a thin region and a thick region, labeled as regions ① and ②, respectively. The color matching between the optical images of regions ① and ③ indicates that the thickness in these regions is close.

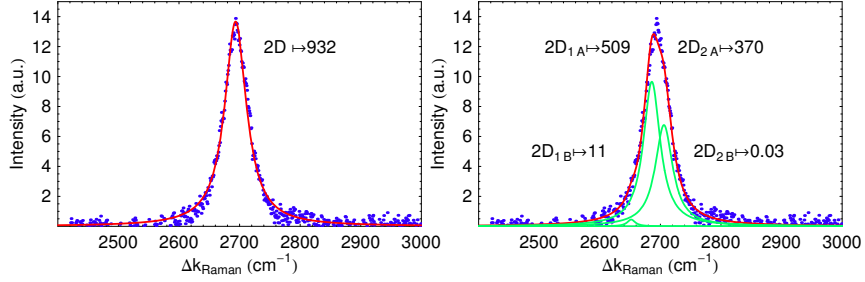


FIGURE 2. Dots: spatially averaged Raman spectra of region ③ (see Fig. 1) subtracted from a nearly flat background due to the presence of gold leads. Left panel—line: best fit of the dots using a Lorentzian function Eq. (1). The number gives the integrated intensity of each peak. Right panel—lines: best fit of the dots using the sum of four Lorentzian functions Eq. (1) using a fixed value for the spacing between the peaks following Table I of Ref. [Ferrari *et al.*(2006)]. The position of the peaks relative to the $2D_{1B}$ peak are 34 cm^{-1} for $2D_{1A}$, 54 cm^{-1} for $2D_{2A}$ and 69 cm^{-1} for $2D_{2B}$.

Raman spectroscopy was performed to determine layer thickness in the three regions using a scanning microscope with 514 nm laser excitation. Figs. 1c and 1d show the width of the $2D$ peak (near 2700 cm^{-1}) as a function of position. The graphitic regions appear clearly on these maps and are perfectly correlated with the optical images. The spectra within the three labeled regions in Figs. 1c and 1d were spatially averaged to obtain a characteristic spectrum for each region. Raman spectroscopy was performed on region ③ after device fabrication and measurement were completed, and after a voltage bias was applied to the device that was sufficiently large to break the contacts (Fig. 4). The presence of the Au leads and contacts on the device, which can be seen as dark lines in Fig. 1d, significantly modifies the Raman spectrum of bare graphene (region ③). Due to this modification, only the $2D$ peak (Fig. 2) could be extracted from the spectrum in this region without significant distortion by subtracting an almost linear background. On Fig. 2, we plot the best fit of this peak using a single Lorentzian function

$$(1) \quad I(\Delta k_{\text{Raman}}) \propto \frac{1}{\Gamma^2/4 + (\Delta k_{\text{Raman}} - \Delta k_{\text{Raman}}^0)^2}.$$

The best fit is obtained for a width $\Gamma = 43 \text{ cm}^{-1}$ and a center at $\Delta k_{\text{Raman}}^0 = 2693 \text{ cm}^{-1}$. The fact that a single Lorentzian fits the $2D$ peak of the device so well indicates that it is made of a single layer of graphene [Ferrari *et al.*(2006), Graf *et al.*(2007)]. For consistency, we also check whether this peak can correspond

to bilayer graphene. In Fig. 2, we plot the best fit of the $2D$ peak assuming it is made of the sum of four Lorentzian peaks following Ref. [Ferrari *et al.*(2006)]. The spacing between these 4 peaks is fixed for bilayers and only the peak widths, peak intensities, and a global offset are fitted. In Fig. 2, it appears that the two components $2D_{1B}$ and $2D_{2B}$ are negligible, which is not the case for bilayer graphene.

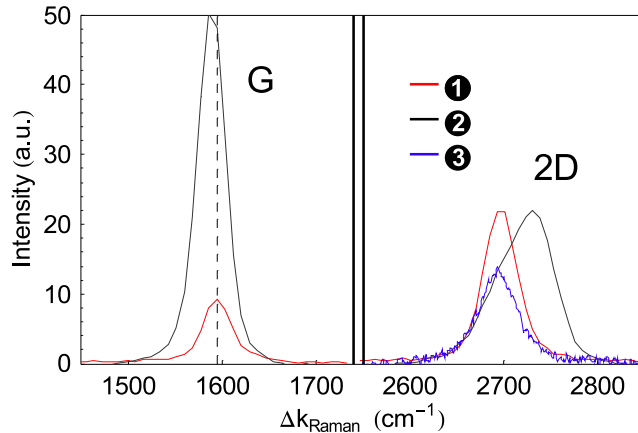


FIGURE 3. Spatially averaged Raman spectra of regions **1**, **2** and **3** (see Fig. 1) for the G (left) and $2D$ (right) peaks. The intensity of the spectrum of region **3** is scaled differently than the two other spectra for clarity.

Furthermore, Graf *et al.* have shown that the ratio of the integrated intensities of the G peak (near 1600 cm^{-1}) to the $2D$ peak gives another measurement of the number of layers [Graf *et al.*(2007)]. Since the Raman spectrum of the graphene in region **3** cannot safely be extracted from the measurement near the G peak due to strong contribution of the Au leads to the Raman signal, it is meaningless to try this analysis on the actual device. However, we performed such a measurement on the nearby graphitic flakes in regions **1** and **2** (Fig. 3), which is informative since optical measurement and the $2D$ Raman peak on regions **1** and **3** are similar. For region **1**, the $G/2D$ ratio is 0.33, which is close to the value obtained in [Graf *et al.*(2007)] for monolayer graphene (0.25 ± 0.04). A single Lorentzian also fits the $2D$ peak in this region well, providing further evidence that it consists of a single layer. By contrast, for region **2**, the $G/2D$ ratio is 1.05 and the $2D$ peak is centered¹ at 2718 cm^{-1} and appears quite broad and non-Lorentzian, suggesting the flake in this region is many layers thick. As a final clue of the flake thickness, one can compare the positions of the G peaks in regions **1** and **2** on Fig. 3. The peak in region **1** is displaced to the right by about 4 cm^{-1} from the peak in region **2** which can only be true if region **1** is a monolayer according to Graf *et al.* [Graf *et al.*(2007)]. All these measurements show that the device investigated in the letter is made of a single layer of graphene.

¹The position of the peaks may depend on the uncontrolled doping of graphene, thus our measurement, the one from Ref. [Graf *et al.*(2007)] and the one from Ref. [Ferrari *et al.*(2006)] give slightly different peak positions. However, the fact that the peaks of regions **1** and **3** sit at the same position which is different from the one of **2** is informative.

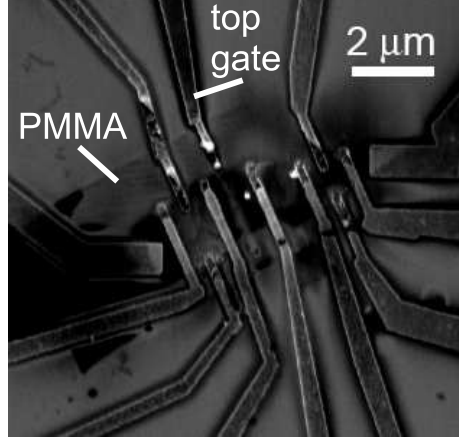


FIGURE 4. Scanning electron microscope image of the fabricated top-gate device. Note the broken Au contacts due to the final destructive measurement on this sample. The graphene sheet appears as the dark region in the center of the contacts.

2. DETERMINATION OF THE DENSITIES IN REGIONS 1 AND 2

As shown in Fig. 2(a) in the letter, the resistance is the sum of a symmetric curve and of a non-zero antisymmetric curve with respect to a sign change of the density n_2 . Therefore, at a fixed value of V_b (or n_1), the voltage $V_t^{(n_2=0)}$ corresponding to $n_2 = 0$ can be slightly different from the voltage V_t^{\max} maximizing the resistance. On Fig. 5, we plot the fitted voltage V_t^{\max} as a function of the back gate voltage V_b . Far from V_b^{\min} , we expect $\partial V_t^{\max}/\partial V_b$ to be constant and equal to the ratio

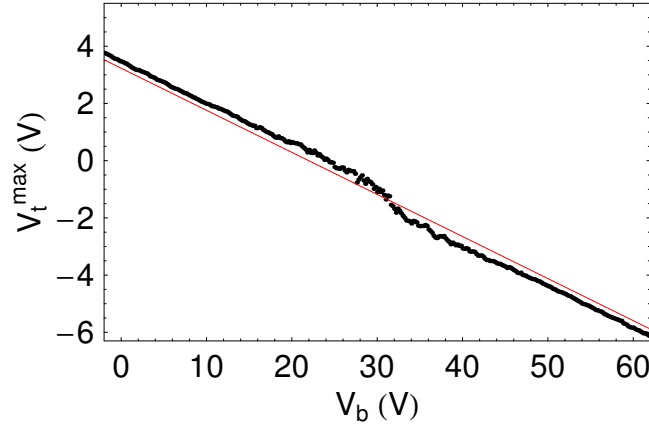


FIGURE 5. Dots: Voltage V_t^{\max} at which the resistance is maximal as a function of the back gate voltage. Line: best fit with a straight line having the same slope at high V_b as the experimental curve.

C_t/C_g between the capacitance per area of the top and back gates (see the letter). This leads to a good estimate of this ratio $C_t/C_g \approx 6.8$. Besides, the shift of the

resistance peak position due to the antisymmetric part should be exactly opposite for opposite values of n_1 . One can see this on Fig. 5 as a global shift towards the positive (resp. negative) V_t when $V_b < V_b^{\min}$ (resp. $V_b > V_b^{\min}$). Therefore, since $n_2 = n_1 + C_t(V_t - V_t^{\min})/e$, the voltage $V_t^{(n_2=0)}$ can be plotted on Fig. 5 as a straight line whose slope is 6.8 and whose position is such that its distance from V_t^{\max} is the same at positive and negative doping n_1 . This gives an estimate for $V_t^{\min} = -1.4$ V.

3. ESTIMATION OF THE MOBILITY

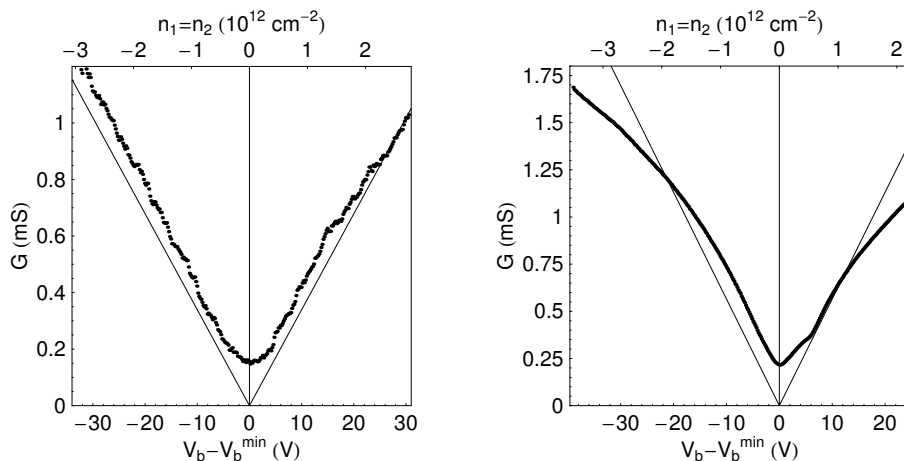


FIGURE 6. Left: conductance measured at 4 K for $n_1 = n_2$ with a line showing a curve of constant mobility $\mu = 1800 \text{ cm}^2 \text{V}^{-1} \text{s}^{-1}$. Right: conductance measured at 77 K for $n_1 = n_2$ with a line showing a curve of constant mobility $\mu = 3000 \text{ cm}^2 \text{V}^{-1} \text{s}^{-1}$.

In order to estimate the mobility of the graphene sheet, we have measured the 4-terminal conductance of the graphene sheet as function of the back gate voltage V_b for a fixed value $V_t = V_t^{\min}$ (see Fig. 6). On the first cool-down of the sample, down to 4 K, the conductance is almost linear in V_b , which indicates that the mobility of the graphene sheet $\mu \equiv d\sigma/dn$ is almost constant at high density, as already observed by several groups [Geim and Novoselov(2007)]. Its slope, together with the known capacitance of the SiO_2 dielectric, allows one to estimate the mobility $\mu \approx 1800 \text{ cm}^2 \text{V}^{-1} \text{s}^{-1}$. After having exposed the sample to air, on the second cool-down of the sample down to 77 K, the conductance as a function of back gate voltage seems to deviate from the linear behavior (Fig. 6). This behavior remains unexplained but could be due to deposits that might have appeared between the two cool-downs.

To determine the effects on electrical transport of embedding graphene in cross-linked PMMA, we measured the two-terminal resistance as a function of V_b on a graphene section covered with cross-linked PMMA and on an uncovered section of the same graphene sheet. All the measurements were performed in liquid Helium at 4 K. Far from the neutrality point – the gate voltage at which average carrier density is zero – the slope $d\sigma/dV_b$ is constant, allowing us to extract a carrier

mobility $\mu \equiv d\sigma/dn = C_b^{-1}d\sigma/dV_b$. We include a constant contact resistance as a fit parameter. The back gate capacitance per area $C_b \approx 14 \text{ nF}\cdot\text{cm}^{-2}$ is inferred from Hall measurements of other graphene flakes on the same oxide layer. The mobility of graphene embedded in the cross-linked PMMA is found to be slightly lower ($\mu \approx 2 \times 10^3 \text{ cm}^2\text{V}^{-1}\text{s}^{-1}$) than in the section not embedded in PMMA ($\mu \approx 3 \times 10^3 \text{ cm}^2\text{V}^{-1}\text{s}^{-1}$). Moreover, the chemical doping of the graphene is different in the two sections, as inferred from the back gate voltage V_b^0 at the minimum conductivity. The value of V_b^0 varies substantially from sample to sample, ranging in similar devices from -1.3 to 250 V , and even changes upon exposure of the graphene to air between cooldowns.

4. MEASUREMENTS AT 77 K

We performed the same measurements as the one described in the letter during a later cool-down at 77 K. We report these measurements in Figs. 7,8. A clear difference between the measurements at the two temperatures comes from the suppression of the universal conductance fluctuations due to an enhanced dephasing rate at 77 K. However, due to the unexplained behavior of the conductance (see Fig. 6), we cannot rule out the contribution of unknown channels of conductance in these measurements.

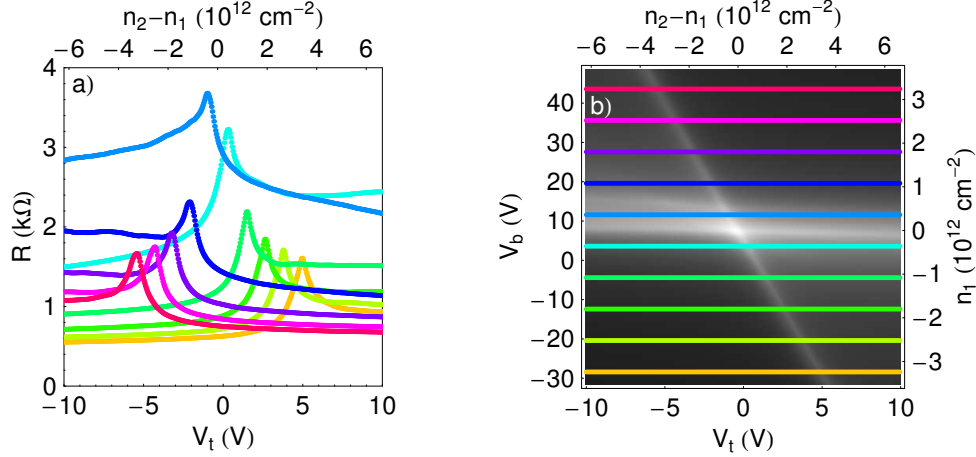


FIGURE 7. a) Resistance across the graphene sample at 77 K as a function of the top gate voltage, for several back gate voltages, each denoted by a different color. b) Greyscale plot of the same resistance as a function of both gate voltages. Traces in a) are cuts along the correspondingly-colored lines.

5. MAGNETO-RESISTANCE MEASUREMENTS

We performed magneto-resistance measurements on the embedded graphene at 4 K in order to estimate the phase coherence length τ_ϕ and the intervalley scattering time τ_i . We have thus measured the resistance of embedded graphene as a function of magnetic field for 17 values of the charge carrier density ranging from $-3.0 \times 10^{12} \text{ cm}^{-2}$ to $-2.3 \times 10^{12} \text{ cm}^{-2}$ between -1 and 1 T (Fig 9). The magneto-resistance

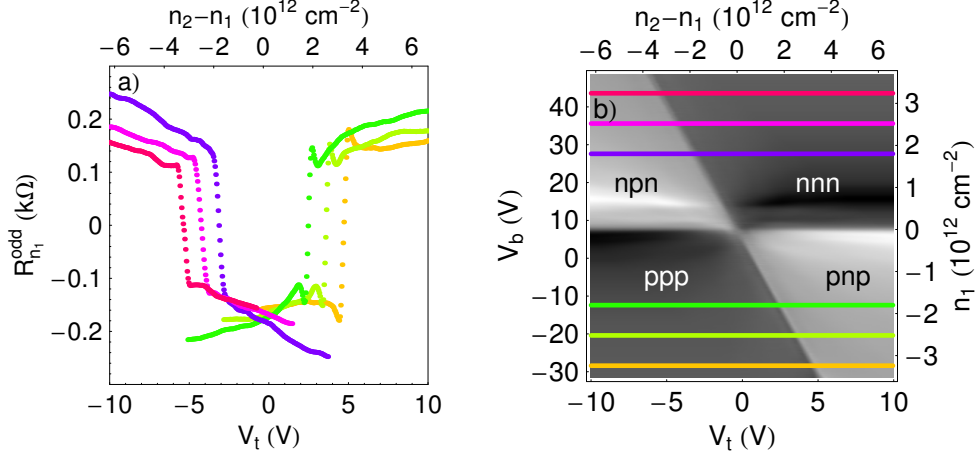


FIGURE 8. a) Odd component of the resistance: the part which depends on the sign of the density n_2 in region 2. Colors correspond to the same values of n_1 as in Fig. 7. b) Greyscale plot of the odd component of the resistance for many values of n_1 . Colored lines are the cuts shown in a).

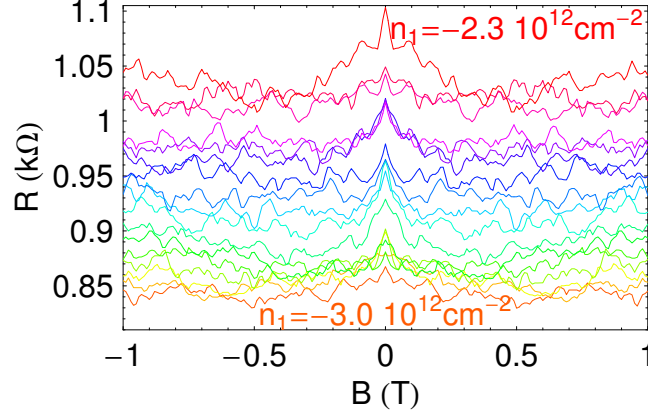


FIGURE 9. Magnetoconductance curves for various densities $n_1 = n_2$ measured at 4K.

fluctuates strongly but is almost perfectly symmetric upon magnetic field reversal, indicating that the fluctuations results from quantum interferences in the electron trajectories. Moreover, a weak localization peak is present at zero magnetic field, but is of the same order of magnitude as the fluctuations. Far from the peak at zero field, one can estimate the average resistance $\langle R \rangle$ for each density and the standard deviation of the magneto-conductance which is $\delta G \equiv (\langle (R - \langle R \rangle)^2 \rangle)^{1/2} / \langle R \rangle^2 \approx 0.2e^2/h$ indicating that the phase coherence length is of the order of or longer than the size of the sample, $L = 1.3 \mu\text{m}$ in this case. Since the universal conductance fluctuations are different at each value of the density, it is tempting to average

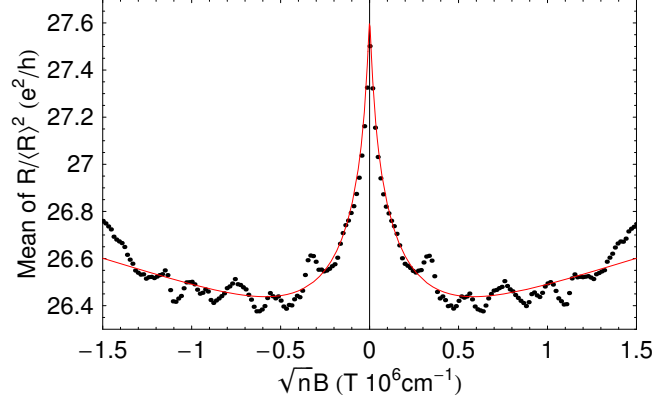


FIGURE 10. Dots: Using the magneto-resistance curves measured at 17 values of the density $n_1 = n_2$ between $-3.0 \times 10^{12} \text{ cm}^{-2}$ to $-2.3 \times 10^{12} \text{ cm}^{-2}$ and measured at 4 K, we plot the average value of the ratio of the resistance R to the square of the mean value of R as a function of $B\sqrt{n}$. This procedure allows one to average out the universal conductance fluctuations so the weak localization peak appears more clearly (see text). Line: theoretical prediction for the same quantity using $L_\varphi = 4 \mu\text{m}$, $L_{i-v} = 150 \text{ nm}$ and $L_\star = 50 \text{ nm}$ in Eq. (2).

them out by averaging all magneto-resistance traces. It is predicted that, without universal conductance fluctuations, the magneto-resistance is [McCann *et al.*(2006)]

$$(2) \quad \frac{\Delta R}{\langle R \rangle^2} = -\frac{e^2}{\pi h} \frac{w}{L} \left[F\left(\frac{B}{B_\varphi}\right) - F\left(\frac{B}{B_\varphi + 2B_{i-v}}\right) - 2F\left(\frac{B}{B_\varphi + B_\star}\right) \right]$$

where

$$(3) \quad F(z) = \ln z + \psi\left(\frac{1}{2} + \frac{1}{z}\right)$$

and, for a mobility μ ,

$$(4) \quad B_\alpha = \frac{1}{2\sqrt{\pi n} \mu L_\alpha}.$$

These equations make explicit the dependence of the magneto-resistance on the density n : the main contribution comes from the term $\langle R \rangle^2$, then each characteristic field B_α grows as $1/\sqrt{n}$ and finally, each critical length L_α itself can depend on n (due to trigonal warping for instance). We can take into account the first two of these effects in order to average out the conductance fluctuations. Indeed, assuming that the lengths L_α are independent of n , one can write the magnetoresistance as

$$(5) \quad \frac{\Delta R}{\langle R \rangle^2}(B, n) = f(B\sqrt{n})$$

therefore averaging $R(B\sqrt{n})/\langle R \rangle^2$ at each value of $B\sqrt{n}$ is the right way to proceed. Plotted in Fig. 10, the resulting curve is in good agreement with the theoretical expression (2) of McCann *et al.* assuming that the phase coherence length is $L_\varphi = 4 \mu\text{m}$, the inter-valley scattering length is $L_{i-v} = 150 \text{ nm}$ and $L_\star = 50 \text{ nm}$.

The large value of L_φ indicates that the inelastic scattering properties in the investigated sample are similar if not weaker than in the samples investigated in Ref. [Morozov *et al.*(2006)]. Besides, the fact that $L_{i-v} < L_\varphi$ is consistent with the graphene lying flat on the substrate [McCann *et al.*(2006), Morozov *et al.*(2006)]. Finally, we show in Fig. 11 the magnetoresistance measured close to zero density to support the discussion on the measurements at finite magnetic field in the letter. Notice how the increase in field seems similar to Fig. 5 of the letter.

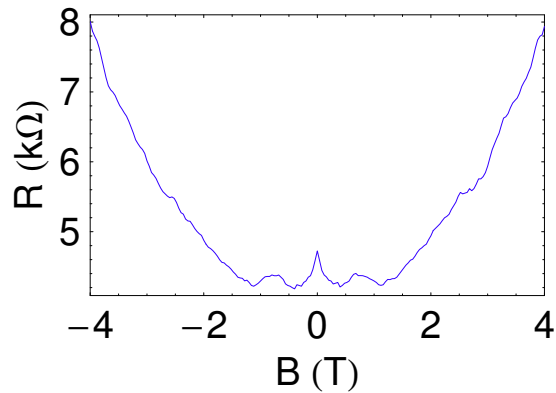


FIGURE 11. Measured magnetoresistance at $V_b = -31.8$ V and $V_t = -1.5$ V, thus close to $n_1 = n_2 = 0$.

REFERENCES

- [Geim and Novoselov(2007)] A. Geim and K. Novoselov, Nat. Mat. **6**, 183 (2007).
[Ferrari *et al.*(2006)] A. C. Ferrari *et al.*, Phys. Rev. Lett. **97**, 187401 (pages 4) (2006).
[Graf *et al.*(2007)] D. Graf *et al.*, Nano Lett. **7**, 238 (2007), ISSN 1530-6984.
[McCann *et al.*(2006)] E. McCann *et al.*, Phys. Rev. Lett. **97**, 146805 (2006).
[Morozov *et al.*(2006)] S. V. Morozov *et al.*, Phys. Rev. Lett. **97**, 016801 (2006).